

# Friction-Induced Transformation from Graphite Dispersed in Esterified Bio-Oil to Graphene

Yufu Xu<sup>1</sup> · Jian Geng<sup>1</sup> · Xiaojing Zheng<sup>2</sup> · Karl D. Dearn<sup>3</sup> · Xianguo Hu<sup>1</sup>

Received: 12 May 2016 / Accepted: 13 June 2016 / Published online: 17 June 2016  
© Springer Science+Business Media New York 2016

**Abstract** Fabricating high-quality graphene with simple methods has aroused considerable interests in recent years. In this paper, graphite was dispersed in esterified bio-oil as a lubricant for steel/gray cast iron friction pairs, and the shear-induced transformation from graphite to graphene was observed. The tribological behavior during this process, including the influence of the normal load and sliding velocity, was investigated. The products formed after sliding were confirmed by Raman spectroscopy, scanning electron microscopy, transmission electron microscopy and X-ray photoelectron spectroscopy. The results showed that friction induces exfoliation, accounting for the transformation from graphite into graphene, and the frictional conditions influence the products. It was also found that high loads and low sliding velocities facilitate the formation of high-quality single-layer graphene during sliding, and high loads and low sliding velocities also contributed to obtaining excellent tribological performance for friction pairs. Friction-induced transformation demonstrates a potentially new strategy for in situ graphene preparation.

**Keywords** Sliding wear · Graphite · Boundary lubrication · Graphene · Bio-oil

## 1 Introduction

Graphene, a two-dimensional layered carbon with  $sp^2$ -bonded carbon, is of considerable interest [1–6] because of its excellent conductivity, high mechanical strength and controllable permittivity, and has many potential applications to energy storage [7], microelectronics [8], lubrication [9], etc. [10]. Many preparation methods have been proposed, including mechanical exfoliation [11], epitaxial growth [12], chemical vapor deposition [13] and reduction of graphene oxide (GO) [14]. Although there have been much progresses in fabricating graphene, the cost and quality of the graphene [15, 16] still remain an issue.

Graphite has been used as a lubricant additive for more than 100 years [17–19]. In the past, most attention has been paid to macroscopic lubricating applications [20–22]. Recently, the friction and wear mechanisms of graphite have been studied and it has been proposed that the inter-lamellar binding forces of graphite were small, which made graphite slippery [23], resulting in a low friction coefficient and low wear. However, few studies have systematically investigated the nature of the debris formed from graphite during sliding [24], although the debris could also influence the tribological behavior. Theoretically, graphite could exfoliate during sliding [25] and form multilayer carbon and potentially also form single-layer graphene under the appropriate conditions. Additionally, it has been shown that graphite as lubricating additives is environment dependent [26] due to the tribochemical reaction between graphite and the chemicals in the surroundings. Therefore, the nature of the dispersing medium is likely to influence the behavior of graphite during sliding.

To date, some work has focused on the tribochemistry and tribo-induced transfer film-forming properties of colloidal dispersion of graphite. However, a relatively small

✉ Yufu Xu  
xuyufu@hfut.edu.cn

<sup>1</sup> Institute of Tribology, School of Mechanical Engineering, Hefei University of Technology, Hefei 230009, China

<sup>2</sup> School of Arts and Media, Hefei Normal University, Hefei 230601, China

<sup>3</sup> School of Mechanical Engineering, University of Birmingham, Edgbaston, Birmingham B152TT, UK

amount of work has explored the friction-induced products, graphene, from graphite dispersed in a fluid [27]. In this work, we chose esterified bio-oil (EBO) as a medium for graphite. EBO, synthesized by converting the acids to esters in the bio-oil, has shown good potential for reducing the corrosive behavior of the crude bio-oils [28–30]. However, the lubricity of EBO still needs to be further improved to be used as a fuel. In our previous work, we found that MoS<sub>2</sub> and graphene had a very good synergetic lubricating effect when dispersed in EBO and could enhance its lubricity significantly [30]. Therefore, using graphite as an additive for EBO not only enables the possibility to improve the friction and wear behavior of EBO, but also allows us to explore the friction-induced exfoliation of graphite. The tribological conditions, including the normal load and sliding speed, were investigated to explore their effects during sliding. The corresponding tribological mechanisms were also investigated.

## 2 Experimental Details

### 2.1 Materials

Flake graphite (purity 99 %) was purchased from Qingdao Haida Graphite Co. Ltd. (Qingdao, China) and was used directly without further purification. Its size ranges from ~120 to ~1400  $\mu\text{m}$ , and the mean particle size is ~500  $\mu\text{m}$  (Fig. 1). A typical micrograph of the edges of the graphite plates is shown in the inset of Fig. 1, indicating a multiple-layer structure of carbon.

EBO was fabricated from crude *Spirulina* algae bio-oil via catalytic esterification [28]. The main chemical components of EBO included esters, ketones, N-containing organics, aldehydes, alkanes and furan. The elemental weight percent of EBO was as follows: C 45.49 %, H 8.57 %, O 44.97 %

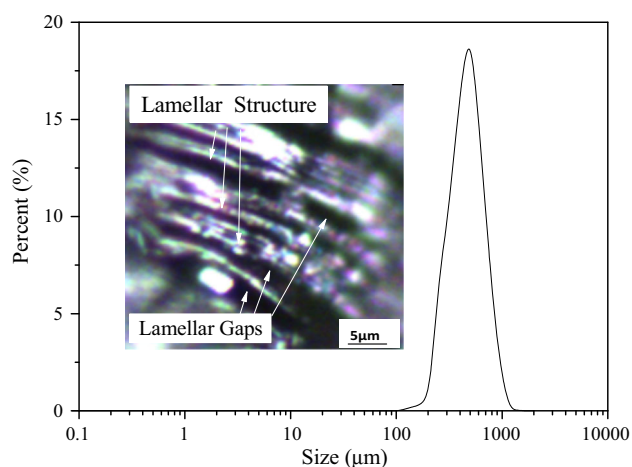


**Fig. 1** Particle-size distribution, micrograph (*inset*) of graphite

and N 0.97 %. The typical physical properties of EBO were as follows: density 866.25 kg m<sup>-3</sup>, viscosity (40 °C) 1.34 mm<sup>2</sup> s, surface tension 24.9 mN m<sup>-1</sup>. More details of its chemical composition and physical properties can be found in our previous work [28].

### 2.2 Tribological Tests

The apparatus that was used to measure friction and wear is shown in Fig. 2. The cylindrical upper friction pair was made from AISI 304 stainless steel with an outside diameter of 32 mm and an inside diameter of 22 mm. To help the graphite to enter into the frictional interfaces and to optimize the yield of products, six grooves were distributed symmetrically around the cylinder. The lower friction pair consisted of a round disk with a diameter of 40 mm and was made from gray cast iron, HT 150 (ASTM-A48 No. 25A). The surface roughness Ra of the surfaces of the cylinder and disk was 0.58 and 0.61  $\mu\text{m}$ , respectively.

In a typical test, 1.0 g of graphite was dispersed in 50 mL of EBO. After ultrasonication for 20 min, the suspension was placed in the oil reservoir of the tribometer. The samples were tested under loads of 100, 150 and 200 N (corresponding to nominal contact pressures of 0.2, 0.3 and 0.4 MPa), using sliding speeds (average speed at the center of the contact annulus) of 0.1, 0.2 and 0.3 m/s. Because of the good compatibility between the graphite and EBO, the micron-sized graphite particles can disperse well in EBO reaching 2 wt% content, using ultrasonic techniques. During the sliding, the rotation of the upper cylinder acts to stir the EBO solution, which facilitates graphite dispersion well in the EBO during the duration of the sliding tests (60 min). Tests were performed at  $30 \pm 4$  °C. After sliding, the samples were washed with acetone. The wear loss was measured from the difference between the weight of the lower friction sample before and

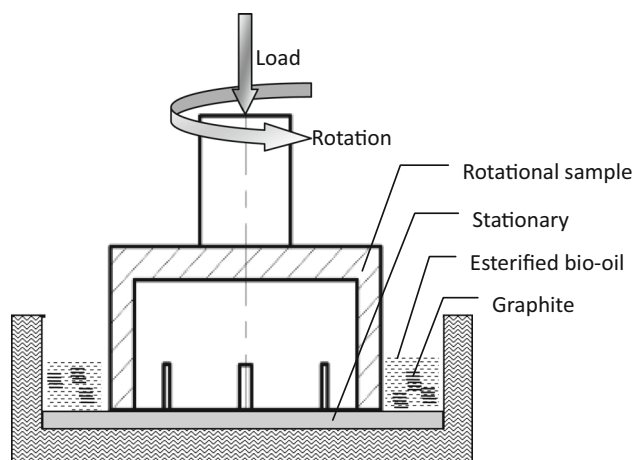


**Fig. 2** Illustration of the end-face tribometer

after sliding, and the wear rate was calculated from the ratio of the wear loss to the sliding distance (average distance at the center of the contact annulus). Each test was repeated twice, and the average values presented as the final results.

After the friction experiments, the liquid products were analyzed by a Agilent Cary 5000 UV–Vis–NIR Spectrophotometer over the range 200–1000 nm. The liquid was filtered, and the solid powder and the friction pairs were washed with acetone and dried at 40 °C in a vacuum-drying oven.

### 2.3 Characterization

The diameters of the solid particles before and after sliding were measured using a Malvern MS-2000 laser particle-size analyzer. Raman spectra of the solid particles before and after sliding were measured using a Horiba Jobin–Yvon LabRAM HR Evolution Raman spectrometer using 532-nm radiation. The microstructure of the solid particles collected from the EBO via filtration and the nature of the rubbed surfaces were observed with a JEOL JSM-6490LV scanning electron microscopy (SEM) by fixing the solid particles onto a silicon substrate with double-sided adhesive tape and were also analyzed using energy-dispersive X-ray spectrometry (EDX). A Hitachi H800 transmission electron microscopy (TEM) was used to observe the microstructure of products with an acceleration voltage of 100 kV. A Thermo ESCALAB 250 X-ray photoelectron spectroscopy (XPS) with Al K $\alpha$  radiation ( $h\nu = 1486.6$  eV) was employed to determine the binding energies of the main element C 1s of the graphite, frictional products and on the worn surfaces.

## 3 Results

### 3.1 Influence of Load on the Lubricant and Sliding Surfaces

The successful fabrication of graphene is confirmed by UV–Vis spectroscopy (Fig. 3), which has been extensively used to analyze the state of the graphene [31, 32]. Sliding experiments were carried out for 60 min at a sliding speed of 0.2 m/s at loads from 100 to 200 N. Following these experiments, the suspended particles and the surfaces were analyzed with other technics. It can be seen from Fig. 3 that the absorption intensity increased after sliding. This suggests that more graphite sheets are present in the solvent, due to exfoliation of graphite during sliding [33]. Furthermore, graphite displays a peak maximum at  $\sim 225$  nm with a shoulder at  $\sim 237$  nm, while, after sliding, peaks redshift slightly to  $\sim 227$  and  $\sim 253$  nm, respectively. This may be caused by the formation of

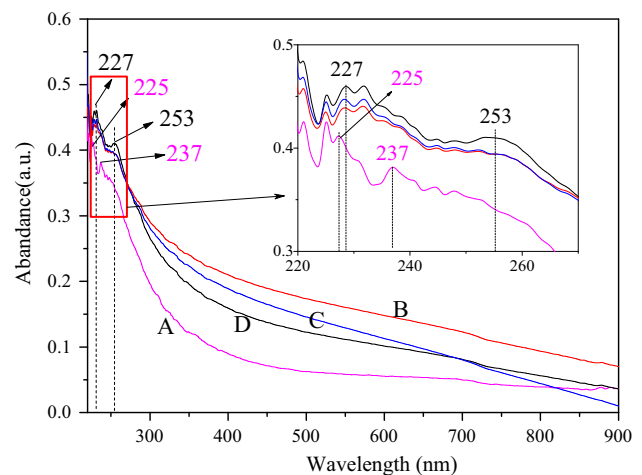


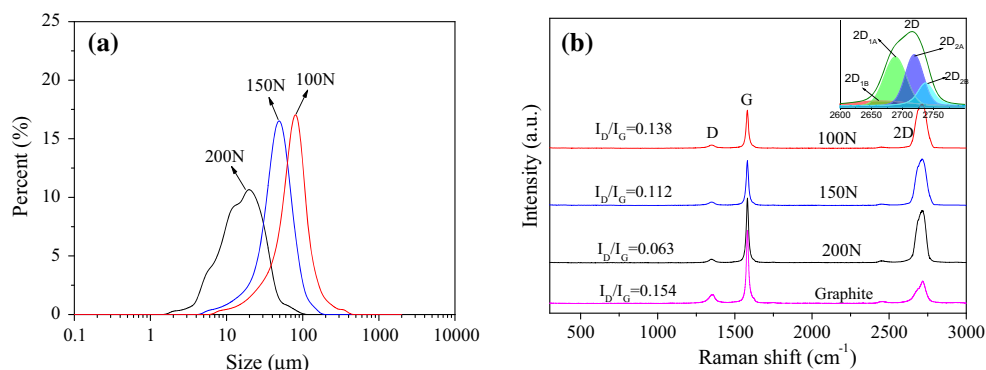
**Fig. 3** UV–Vis spectra of graphite dispersed in EBO before and after sliding under different loads

auxochromic groups such as  $-\text{OH}$  owing to friction oxidation [34] and also indicates that the  $\pi$ -conjugation of graphene sheets is restored due to the formation of some new  $sp^2$  carbon bonds in the triboaction [32].

Figure 4 shows the particle-size distribution and Raman spectra of the lubricant graphite sliding under different loads. As shown in Fig. 4a, the particle size of the products decreased with increasing load, indicating that higher loads contributed to the exfoliation of graphite. Raman spectroscopy is considered as a very effective technique for investigating the nature of the graphene [35]. The Raman spectrum (Fig. 4b) shows the  $D$  ( $\sim 1354$   $\text{cm}^{-1}$ ),  $G$  ( $\sim 1580$   $\text{cm}^{-1}$ ) and  $2D$  ( $\sim 2713$   $\text{cm}^{-1}$ ) bands of wear products and graphite. The  $D$  peak results from the breathing mode of the  $sp^2$ -C atoms, which is induced by structural disorder defects [36]. The intensity ratio,  $I_D/I_G = 0.154$ , suggests a low degree of disorder of the graphite. It can be seen from Fig. 4b that the  $D$ ,  $G$  and  $2D$  bands of the products were detected, and the  $I_D/I_G$  ratio decreased with increasing load, suggesting that higher loads helped to reduce the defects in the graphene. A possible explanation is that higher loads contributed to the exfoliation of graphite, and the exfoliated graphite sheets more easily adsorbed on the rubbing surfaces, which prevents the graphene from directly contacting rubbing surfaces and being destroyed [24, 37, 38]. Meanwhile, all the  $2D$  peaks of the wear products (inset of Fig. 4b) are clearly different from those of graphite and can be resolved into four components, consisting of  $2D_{1B}$ ,  $2D_{1A}$ ,  $2D_{2A}$  and  $2D_{2B}$ ; the intensity of  $2D_{1A}$  and  $2D_{2A}$  is higher than those of the  $2D_{1B}$  and  $2D_{2B}$ , indicating the graphene contains no more than five layers. The intensity of  $2D$  band is close to that of the  $G$  band, suggesting that the main products are bilayer graphene [39].

Micrographs of the particles in the lubricant after sliding under different loads are shown in Fig. 5. There is a clear

**Fig. 4** **a** Particle-size distribution and Raman spectrum of **b** graphene transformed from graphite after sliding under different loads



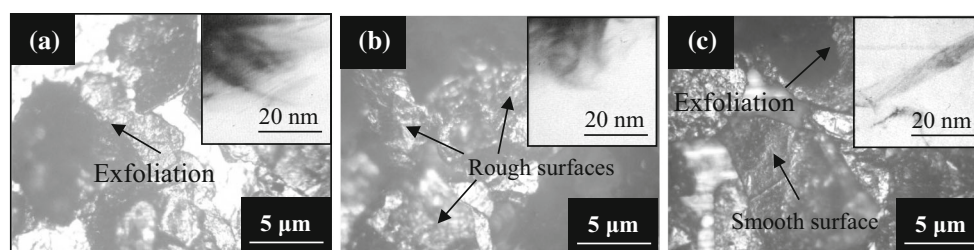
exfoliation of the graphene sheets seen in Fig. 5a. The graphene sheets in Figs. 5a, b and c maintain their original laminated structure from graphite, with diameters between  $\sim 4$  and  $\sim 20$   $\mu\text{m}$ , which are similar to the results reported by Lin et al. [40]. Typical few-layer structures can be seen clearly in the amplified TEM images. In addition, with an increase in load, the graphene had a smaller particle size. These trends are in accord with the particle-size distribution in Fig. 4a. The detailed diameters in Fig. 5 are different from those in Fig. 4a because of the different analysis methods. Only several particles can be observed in SEM images, while the total statistical results can be obtained by using laser particle-size analysis.

Figure 6 presents the friction coefficient and wear rate of the stationary sample lubricated with EBO and graphite dispersed in EBO under different loads. Shown in Fig. 6a is the average friction coefficient of EBO with graphite ( $0.08 \pm 0.01$ ), which was much lower than that of pure EBO ( $0.12 \pm 0.02$ ), both under a load of 100 N, and it decreased by more than 28 %, indicating that graphite had a beneficial lubricating role. Furthermore, the EBO with graphite had a shorter run-in period than pure EBO. This may be due to the exfoliation of graphite producing small graphene sheets that fill in the grooves on the surfaces and quickly form a tribofilm [41]. The run-in period also decreased with increasing load. The steady-state friction coefficient for EBO with graphite decreased from  $0.08 \pm 0.01$  to  $0.06 \pm 0.01$  with an increase in load from

100 to 200 N. This may be because higher loads lead to larger plastic deformation of the stationary sample, increasing the real contact area, which causes more graphene sheets to adsorb on the rubbing surfaces, to decrease the contact stress of the friction pairs [42], and then to decrease the coefficient of friction.

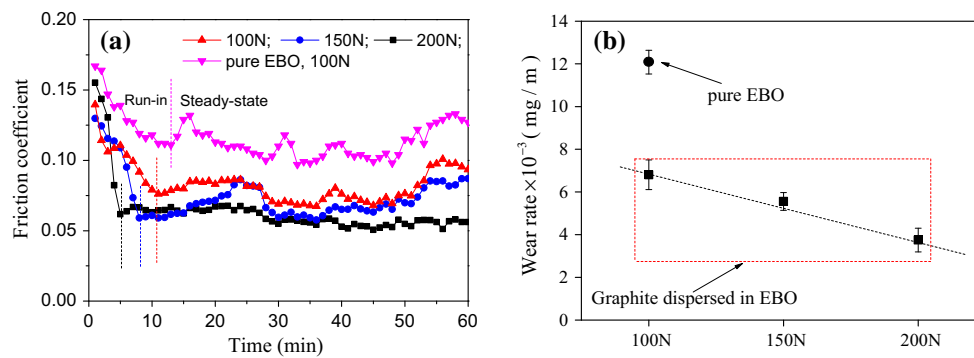
From Fig. 6b, it can be seen that the wear rate per meter of the stationary sample lubricated by EBO with graphite decreased by more than 44 % compared to that lubricated by pure EBO. This might be connected with the rheology of the EBO with and without graphite particles. EBO with additives had a higher viscosity than pure EBO, which resulted in graphite particles being more likely to be adsorbed on the rubbing surfaces and prevent them from wearing. The wear rate decreases almost linearly from  $(6.8 \pm 0.7) \times 10^{-3}$  to  $(3.8 \pm 0.6) \times 10^{-3}$  mg/m with an increase in load from 100 to 200 N when lubricated with EBO containing graphite.

Figure 7 shows micrographs of the worn surfaces of the stationary sample that had been lubricated with EBO, and EBO with graphite, under different loads. The surfaces lubricated by EBO alone showed clear delamination wear [43], while, with added graphite, wear was reduced and the surface exhibited some spalling pits under a load of 100 N. Adhesive material and furrows occurred when the load increased to 150 N. The surfaces became much smoother with only some light furrows under a load of 200 N, indicating mild wear. According to these micrographs and



**Fig. 5** Micrographs of graphene (insets are TEM images) transformed from graphite after sliding under different loads: **a** 100 N, **b** 150 N and **c** 200 N





**Fig. 6** **a** Friction coefficient and **b** wear rate of stationary sample lubricated with EBO and graphite dispersed in EBO under different loads (sliding speed: 0.2 m/s, sliding time: 60 min)

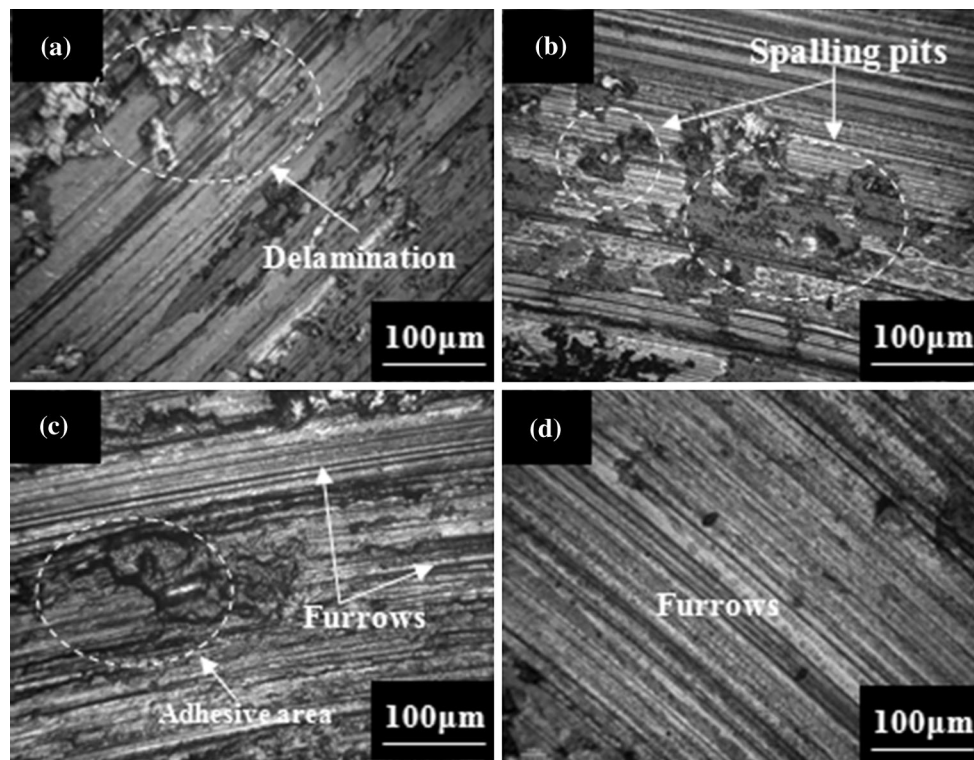


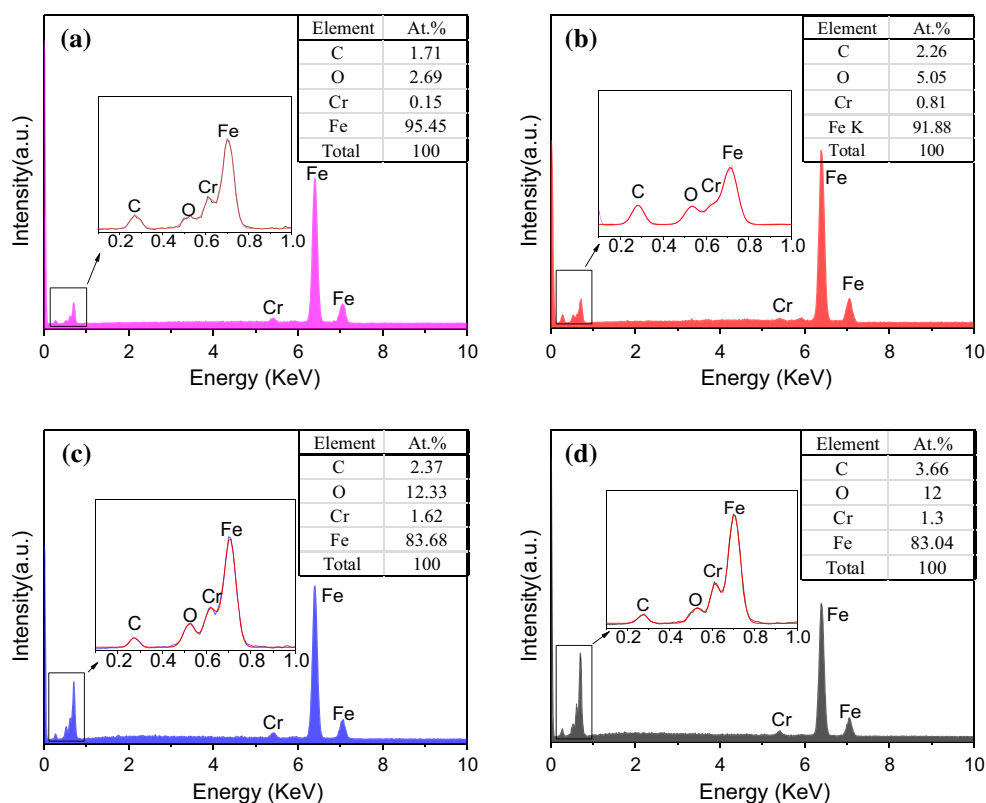
**Fig. 7** Micrographs of worn surfaces of stationary sample lubricated with EBO (**a**) and graphite dispersed in EBO under different loads: **b** 100 N, **c** 150 N and **d** 200 N

tribological data above, the four wear types in Fig. 7 are classified as delamination wear, spalling wear, adhesive wear and mild wear, respectively. That is, the graphite as EBO additives could prevent the rubbed surfaces from delaminating and further reduce wear under higher loads. Higher loads produced much smoother worn surfaces, which agrees well with the decrease in wear rate under higher loads in Fig. 6. The reasons will be further discussed in the following section.

Figure 8 displays the EDX results of the worn surfaces of the stationary sample lubricated with EBO, and EBO

with graphite, under different loads. It can be seen that, for pure EBO lubrication (Fig. 8a), the carbon and oxygen on the worn surfaces likely come from EBO decomposition [28], while the chromium might originate from transfer from the AISI 304 stainless-steel counterface [44]. The rubbed surfaces lubricated with EBO with graphite (Fig. 8b) had higher contents of carbon and oxygen than that lubricated by the pure EBO (Fig. 8a), indicating that, during the frictional process, the graphite can be exfoliated into graphene, and then, some of graphene can react with the worn surfaces to form a complex tribofilm [45].

**Fig. 8** EDX of worn surfaces of stationary sample lubricated with EBO (a) and graphite dispersed in EBO under different loads: **b** 100 N, **c** 150 N and **d** 200 N



Furthermore, the rate of this triboreaction increased at higher loads (Figs. 8b–d) since larger amounts of carbon were detected. That is, friction-induced exfoliation causes graphite to transform into graphene and then adsorb or react on the rubbing surfaces. Moreover, higher loads deposit more graphene and form thicker tribofilms, decreasing the friction coefficient and wear rate in accord with the friction and wear results in Figs. 6, 7. Therefore, in the following section a higher load of 250 N was chosen for investigating the influence of sliding speed.

### 3.2 Influence of Sliding Speed on the Lubricant and Sliding Surfaces

Figure 9 shows the UV–Vis spectra of graphite dispersed in EBO before and after sliding at different speeds with a load of 250 N. After sliding, both the peak maximum and the shoulder shifted to higher wavelengths,  $\sim 232$  and  $\sim 253$  nm, respectively, indicating that the  $\pi$ -conjugation within the graphene increased [32]. Moreover, the absorbance increased with increasing sliding speed, indicating that higher sliding speeds are helpful for the formation of more auxochromic groups including hydroxyl groups due to the enhancement of the tribo-oxidation reaction [46].

Figure 10 displays the particle-size distribution and Raman spectra of the graphite particles in the liquid after sliding at different sliding speeds. As can be seen from

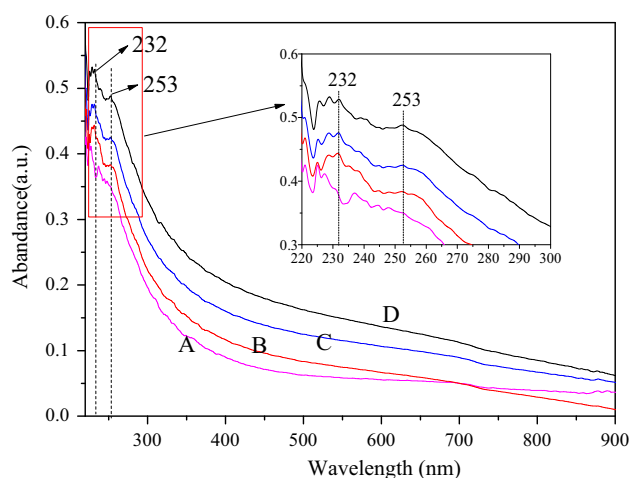
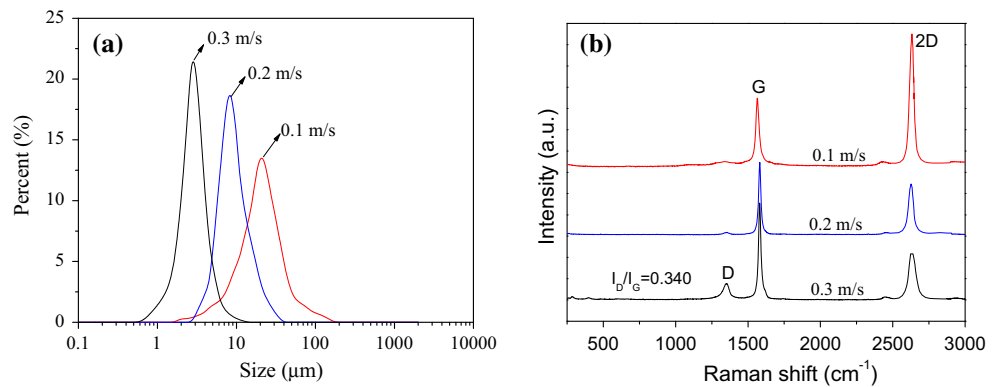


**Fig. 9** UV–Vis spectra of graphite dispersed in EBO before and after sliding under different sliding speeds (load: 250 N, sliding time: 60 min)

Fig. 10a, the particle size decreased and distribution became narrower with an increase in sliding speed. This may be because higher speeds facilitate exfoliation of the graphite into smaller pieces. Figure 10b shows that single-layer graphene can be obtained at a speed of 0.1 m/s, since the intensity of single 2D peak is twice that of G peak [39]. The main components of the products are bilayer and few-layer graphene with some graphite at speeds of 0.2 and

**Fig. 10** **a** Particle-size distribution and **b** Raman spectra of graphene transformed from graphite after sliding under different sliding speeds



0.3 m/s, respectively, because the intensity of 2D band is  $\sim 0.9$  and  $\sim 0.6$  times that of the G band [47]. The D band peaks disappeared at sliding velocities of 0.1 and 0.2 m/s, but reappeared again at 0.3 m/s, indicating high-quality single-layer graphene could be obtained [39] at low sliding speed of 0.1 m/s, but the defects increased in the carbon layer of the products at higher speed.

Figure 11 displays micrographs of the particles in the fluid after sliding at different speeds. As shown, large slice structures with wrinkles in the graphene remained at low sliding speeds, while higher sliding speed led to exfoliated products in small pieces. These SEM image results agree with both the Raman spectra in Fig. 10b and TEM images.

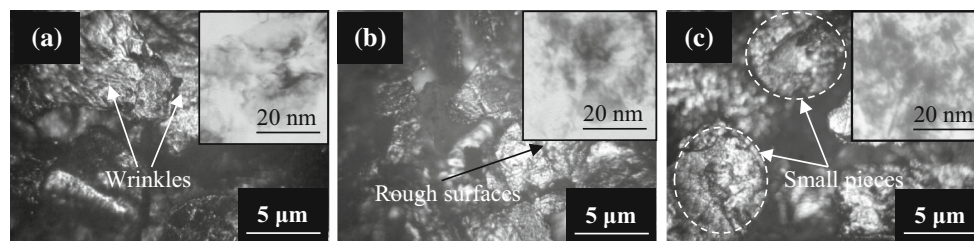
The friction and wear behavior of the contacts lubricated with graphite dispersed in EBO at different sliding speeds are shown in Fig. 12. Figure 12a indicates that, during the run-in and initial stages, the friction coefficient decreased with an increase in sliding speed. However, in the follow-up stage, the friction coefficient at a high sliding speed (0.3 m/s) is higher than that at a low sliding speed (0.1 m/s). This may be because high sliding speeds contributed to the initial formation of a tribofilm, but it then destroys the tribofilm after long sliding times [42]. Figure 12b shows that the wear rate increased slightly with an increase of sliding speed.

Figure 13 shows micrographs of the worn surfaces of the stationary sample lubricated with graphite dispersed in EBO at different sliding speeds. It can be noted that there were some thin and dense furrows on the worn surfaces at low speed (Fig. 13a), suggesting it had only slight wear.

The surface roughness increased and the wear furrows became wider with an increase in sliding speed (Figs. 13b, c), indicating that the wear types belong to mild wear and severe wear, respectively [48].

Figure 14 shows the EDX results of the worn surfaces of the stationary sample lubricated with graphite dispersed in EBO at different sliding speeds. As shown in the figures, the relative contents of carbon and oxygen decreased with an increase in sliding speed, indicating that the tribofilm became thinner under high sliding speed. The element chromium resulted from the upper friction pair owing to material transfer during sliding [49]. The iron from the substrate can also be detected. In addition, silicon was found on the worn surfaces at high sliding speeds, which came from the gray cast iron substrate, confirming that high sliding speeds are detrimental to the formation of single-layer graphene and may destroy the tribofilm.

In order to further study the sliding process, XPS spectra of C1 s were measured with the raw material, frictional products and worn surfaces. The results are shown in Fig. 15. As shown, there are some defects and oxides in the raw material graphite since the  $Csp^3$  and C–O bond were detected clearly. However, no oxides and few  $Csp^3$  were found in frictional products, and the content of  $Csp^2$  is more than 91 %, indicating a high quality of graphene. Simultaneously, more content of  $Csp^2$  and few content of  $Csp^3$  and C–O bond were measured on the worn surfaces than those of raw material, suggesting that adsorbed or squeezed graphene on the frictional surfaces might play an important antifriction and antiwear role.



**Fig. 11** Micrographs of graphene (*insets* are TEM images) transformed from graphite after sliding under different sliding speeds: **a** 0.1 m/s, **b** 0.2 m/s and **c** 0.3 m/s

**Fig. 12** **a** Friction coefficient and **b** wear rate of stationary sample lubricated with graphite dispersed in EBO under different sliding speeds (load: 250 N, sliding time: 60 min)

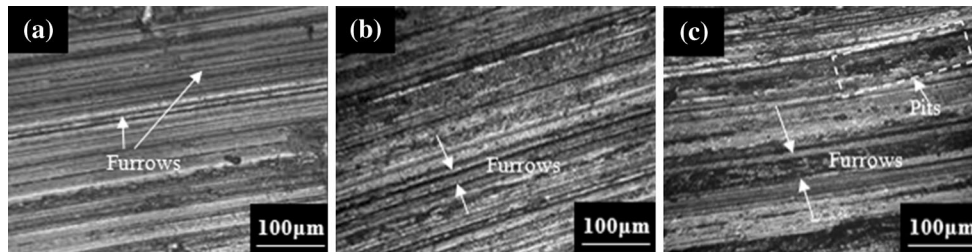
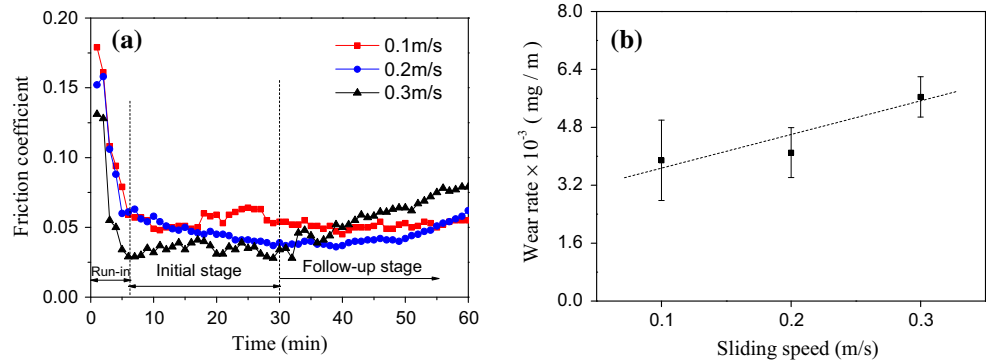


**Fig. 13** Micrographs of worn surfaces of stationary sample lubricated with graphite dispersed in EBO under different sliding speeds: **a** 0.1 m/s, **b** 0.2 m/s and **c** 0.3 m/s

**Fig. 14** EDX of worn surfaces of stationary sample lubricated with graphite dispersed in EBO under different sliding speeds: **a** 0.1 m/s, **b** 0.2 m/s and **c** 0.3 m/s

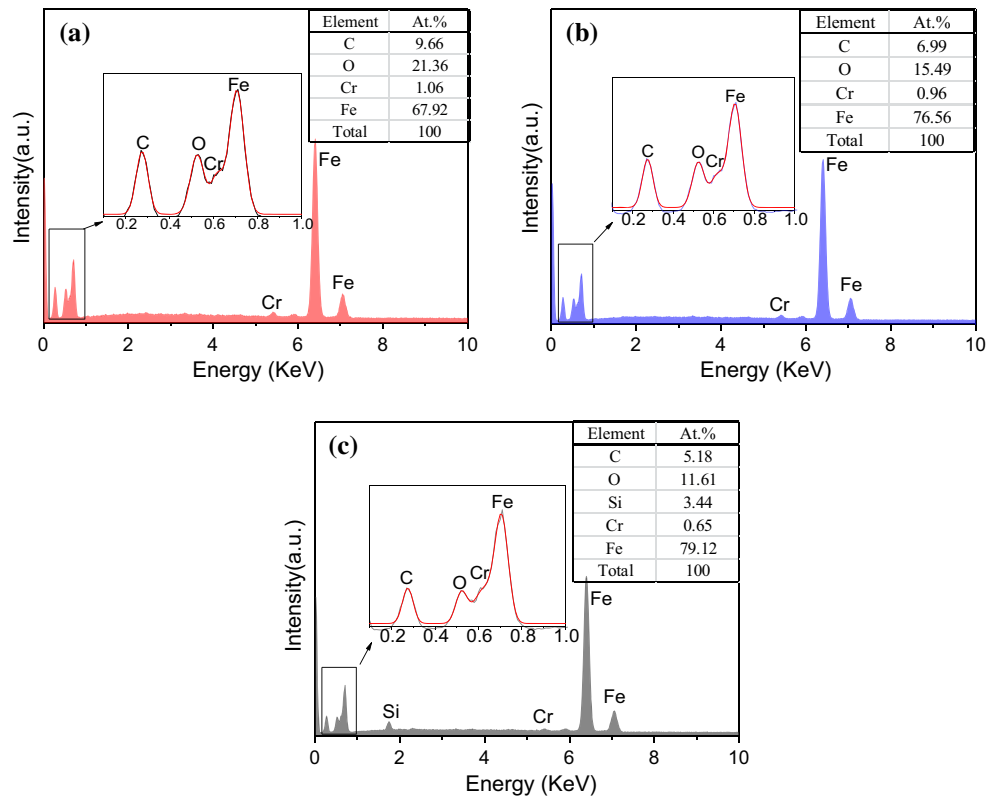
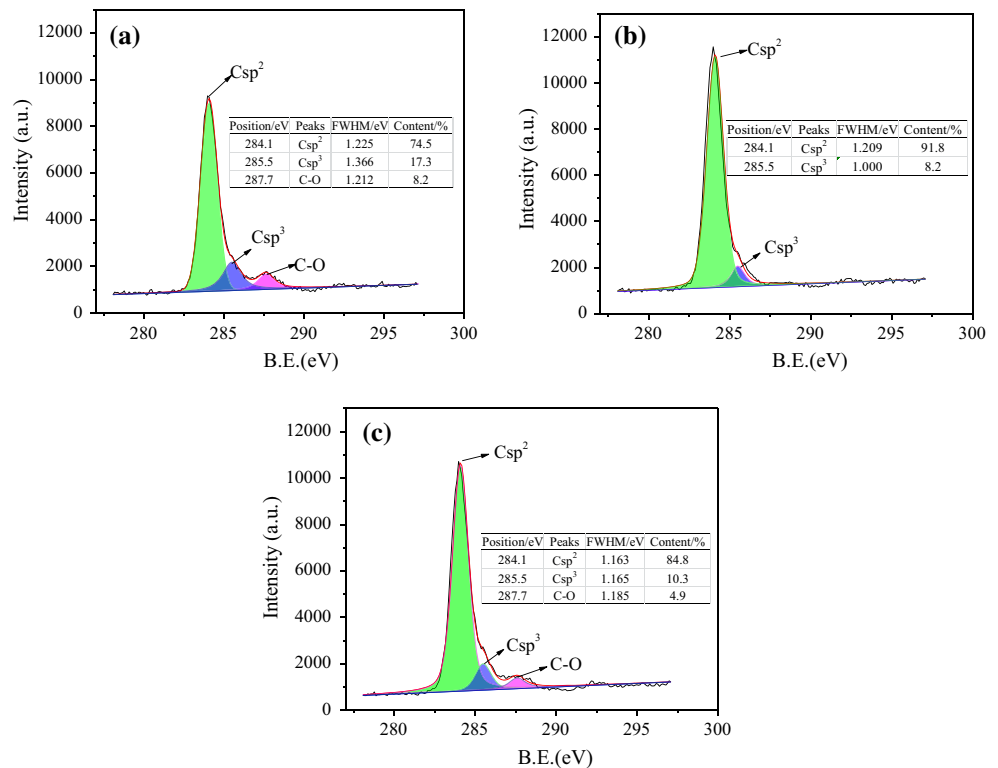




**Fig. 15** XPS spectra of C1 s of **a** graphite, **b** frictional products and **c** worn surfaces under conditions as follows: sliding speed: 0.1 m/s, load: 250 N; sliding time: 60 min



## 4 Discussion

According to all the experimental results above, a schematic explanation of the tribological mechanisms is shown in Fig. 16. As shown, under sliding conditions of loads between 100 and 250 N and sliding speeds between 0.1 and 0.3 m/s, the suspended graphite was transformed into multi-/single-layer graphene. This was confirmed by the measured  $I_D/I_G$  ratios in the Raman spectra in Figs. 4b and 10b. The graphene then forms a thin tribofilm on the rubbed surfaces, decreasing the friction and wear, which was verified by the EDX data in Figs. 8 and 14. According to Berman et al. [50], passivation effects might be the main reason for the friction-reducing and antiwear properties of graphene, and here the dispersed medium bio-oil has affected the tribological transformation to graphene from graphite. With an increase in load, shear effects were enhanced and smaller graphene particles were obtained (Fig. 4a), and more graphene sheets remained on the rubbed surfaces, which led to a thicker tribofilm (Fig. 8) acting as a solid lubricating film [51] on the surfaces. Therefore, the graphene from graphite alleviated the material removal rate and resulted in lower friction with increasing loads between steel/gray cast iron pairs.

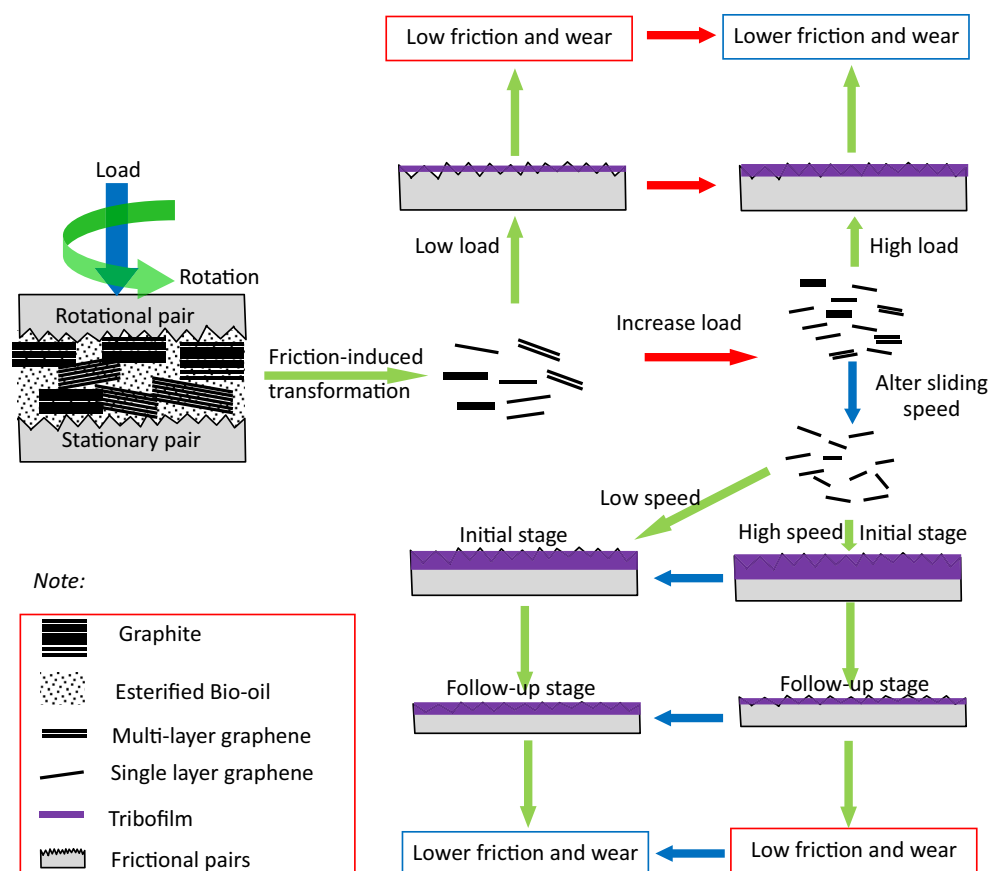
Changing sliding speeds significantly influenced the products. On the one hand, at high speeds smaller graphene sheets were formed (shown in Fig. 10a). In the initial stage, smaller graphene sheets more easily formed a thick

tribofilm on the surface [52], resulting in lower friction at this stage as shown in Fig. 12a. However, during sliding, the graphite and graphene remained on the rubbing surfaces for a shorter time at high sliding speeds than those with lower sliding speeds [30]. In addition, at higher sliding speeds, sliding led to more defects in the carbon layer of the products (Fig. 10b) and it was much easier to destroy the tribofilm on the rubbing surfaces. This can be inferred from the micrographs of the worn surfaces in Fig. 13 and the elemental contents in Fig. 14. On the other hand, at low speeds, according to the elemental contents analysis, although the tribofilm was not very thick, high-quality single-layer graphene could be maintained on the surfaces for a longer time than under high speed due to the weak polishing role of friction pairs at low speeds [53], which resulted in lower friction and wear at the end of sliding.

## 5 Conclusions

Graphite was dispersed in EBO and played a beneficial lubricating role between an upper rotational and lower stationary steel/gray cast iron pair. It was found that friction-induced transformation is an effective method to fabricate graphene from graphite. Higher loads and lower sliding velocities contribute to the formation of high-quality single-layer graphene during sliding. Exfoliation was induced by sliding to transform graphite into graphene,

**Fig. 16** Schematic explanation of tribological mechanisms



which then adsorbed or reacted on the rubbing surfaces to prevent the material from severe wear. Higher loads produced more graphene and a thicker tribofilm, which decreased the friction coefficient and wear rate. During the initial stage, higher sliding speeds help to form a thicker tribofilm composed of graphene and other components on the rubbing surfaces, which results in low friction and wear. During the follow-up stage, the tribofilm is easily destroyed, so that the friction and wear of the samples increase. The single-layer graphene formed under low sliding speed remains on the rubbing surfaces for a longer time to contribute to lower friction and wear of the friction pairs.

**Acknowledgments** We sincerely appreciate Prof. Wilfred T. Tysoe of University of Wisconsin–Milwaukee for giving helpful revisions and constructive suggestions. This work was supported by the National Natural Science Foundation of China (Grant No. 51405124), the China Postdoctoral Science Foundation (Grant No. 2015T80648 & 2014M560505), the Anhui Provincial Natural Science Foundation (Grant No. 1408085ME82) and the Tribology Science Fund of State Key Laboratory of Tribology (Grant No. STKLKF15A05).

## References

- Zhang, Y., Tan, Y.-W., Stormer, H.L., Kim, P.: Experimental observation of the quantum Hall effect and Berry's phase in graphene. *Nature* **438**, 201–204 (2005)
- Li, X., Cai, W., An, J., Kim, S., Nah, J., Yang, D., Piner, R., Velamakanni, A., Jung, I., Tutuc, E.: Large-area synthesis of high-quality and uniform graphene films on copper foils. *Science* **324**, 1312–1314 (2009)
- Kostarelos, K., Novoselov, K.S.: Exploring the interface of graphene and biology. *Science* **344**, 261–263 (2014)
- Bonaccorso, F., Colombo, L., Yu, G., Stoller, M., Tozzini, V., Ferrari, A.C., Ruoff, R.S., Pellegrini, V.: Graphene, related two-dimensional crystals, and hybrid systems for energy conversion and storage. *Science* **347**, 1246501 (2015)
- Le, T.X.H., Bechelany, M., Lacour, S., Oturan, N., Oturan, M.A., Cretin, M.: High removal efficiency of dye pollutants by electron-Fenton process using a graphene based cathode. *Carbon* **94**, 1003–1011 (2015)
- Novoselov, K.S., Geim, A.K., Morozov, S., Jiang, D., Zhang, Y., Dubonos, S.A., Grigorieva, I., Firsov, A.: Electric field effect in atomically thin carbon films. *Science* **306**, 666–669 (2004)
- Raccichini, R., Varzi, A., Passerini, S., Scrosati, B.: The role of graphene for electrochemical energy storage. *Nat. Mater.* **14**, 271–279 (2015)
- Wu, K.-H., Cheng, H.-H., Mohammad, A.A., Blakey, I., Jack, K., Gentle, I.R., Wang, D.-W.: Electron-beam writing of deoxygenated micro-patterns on graphene oxide film. *Carbon* **95**, 738–745 (2015)
- Yao, J., Shi, X., Zhai, W., Ibrahim, A.M.M., Xu, Z., Chen, L., Zhu, Q., Xiao, Y., Zhang, Q., Wang, Z.: The enhanced tribological properties of NiAl intermetallics: combined lubrication of multilayer graphene and WS<sub>2</sub>. *Tribol. Lett.* **56**, 573–582 (2014)
- Kay, L., Porter, A.L., Youtie, J., Rafols, I., Newman, N.: Mapping graphene science and development: focused research with multiple application areas. *J. Am. Soc. Inf. Sci. Tech.* **41**, 22–25 (2015)

11. Yi, M., Shen, Z.: A review on mechanical exfoliation for the scalable production of graphene. *J. Mater. Chem. A* **3**, 11700–11715 (2015)
12. Tetlow, H., De Boer, J.P., Ford, I., Vvedensky, D., Coraux, J., Kantorovich, L.: Growth of epitaxial graphene: theory and experiment. *Phys. Rep.* **542**, 195–295 (2014)
13. Strudwick, A.J., Weber, N.E., Schwab, M.G., Kettner, M., Weitz, R.T., Wünsch, J.R., Müllen, K., Sachdev, H.: Chemical vapor deposition of high quality graphene films from carbon dioxide atmospheres. *ACS Nano* **9**, 31–42 (2014)
14. Chua, C.K., Pumera, M.: Chemical reduction of graphene oxide: a synthetic chemistry viewpoint. *Chem. Soc. Rev.* **43**, 291–312 (2014)
15. Novoselov, K.S., Fal, V., Colombo, L., Gellert, P., Schwab, M., Kim, K.: A roadmap for graphene. *Nature* **490**, 192–200 (2012)
16. Kuila, T., Bose, S., Hong, C.E., Uddin, M.E., Khanra, P., Kim, N.H., Lee, J.H.: Preparation of functionalized graphene/linear low density polyethylene composites by a solution mixing method. *Carbon* **49**, 1033–1037 (2011)
17. Barham, G.: Good and bad lubricants. *J. Am. Soc. Nav. Eng.* **27**, 694–697 (1915)
18. Gillett, H.W.: Analyses and friction tests of lubricating greases. *Ind. Eng. Chem.* **1**, 351–360 (1909)
19. Mabery, C.F.: Lubrication with oils, and with colloidal graphite. *Ind. Eng. Chem.* **5**, 717–723 (1913)
20. Shaji, S., Radhakrishnan, V.: Analysis of process parameters in surface grinding with graphite as lubricant based on the Taguchi method. *J. Mater. Process. Technol.* **141**, 51–59 (2003)
21. Alberts, M., Kalaitzidou, K., Melkote, S.: An investigation of graphite nanoplatelets as lubricant in grinding. *Int. J. Mach. Tool Manuf.* **49**, 966–970 (2009)
22. Suresh Kumar Reddy, N., Venkateswara Rao, P.: Performance improvement of end milling using graphite as a solid lubricant. *Mater. Manuf. Process.* **20**, 673–686 (2005)
23. Kumar, N., Dash, S., Tyagi, A.K., Raj, B.: Super low to high friction of turbostratic graphite under various atmospheric test conditions. *Tribol. Int.* **44**, 1969–1978 (2011)
24. Mungse, H.P., Kumar, N., Khatri, O.P.: Synthesis, dispersion and lubrication potential of basal plane functionalized alkylated graphene nanosheets. *RSC Adv.* **5**, 25565–25571 (2015)
25. Toyoda, M., Inagaki, M.: Heavy oil sorption using exfoliated graphite: new application of exfoliated graphite to protect heavy oil pollution. *Carbon* **38**, 199–210 (2000)
26. Marks, N.: Generalizing the environment-dependent interaction potential for carbon. *Phys. Rev. B* **63**, 035401 (2000)
27. León, V., Rodriguez, A.M., Prieto, P., Prato, M., Vázquez, E.: Exfoliation of graphite with triazine derivatives under ball-milling conditions: preparation of few-layer graphene via selective noncovalent interactions. *ACS Nano* **8**, 563–571 (2014)
28. Xu, Y., Zheng, X., Hu, X., Dearn, K.D., Xu, H.: Effect of catalytic esterification on the friction and wear performance of bio-oil. *Wear* **311**, 93–100 (2014)
29. Xu, Y., Hu, X., Yuan, K., Zhu, G., Wang, W.: Friction and wear behaviors of catalytic methylesterified bio-oil. *Tribol. Int.* **71**, 168–174 (2014)
30. Xu, Y., Peng, Y., Dearn, K.D., Zheng, X., Yao, L., Hu, X.: Synergistic lubricating behaviors of graphene and MoS<sub>2</sub> dispersed in esterified bio-oil for steel/steel contact. *Wear* **342**, 297–309 (2015)
31. Wang, G., Shen, X., Wang, B., Yao, J., Park, J.: Synthesis and characterisation of hydrophilic and organophilic graphene nanosheets. *Carbon* **47**, 1359–1364 (2009)
32. Li, D., Muller, M.B., Gilje, S., Kaner, R.B., Wallace, G.G.: Processable aqueous dispersions of graphene nanosheets. *Nat. Nanotechnol.* **3**, 101–105 (2008)
33. Liang, S., Shen, Z., Yi, M., Liu, L., Zhang, X., Ma, S.: In-situ exfoliated graphene for high-performance water-based lubricants. *Carbon* **96**, 1181–1190 (2016)
34. Han, H., Gao, Y., Zhang, Y., Du, S., Liu, H.: Effect of magnetic field distribution of friction surface on friction and wear properties of 45 steel in DC magnetic field. *Wear* **328**, 422–435 (2015)
35. Ferrari, A.C., Meyer, J.C., Scardaci, V., Casiraghi, C., Lazzeri, M., Mauri, F., Piscanec, S., Jiang, D., Novoselov, K.S., Roth, S., Geim, A.K.: Raman spectrum of graphene and graphene layers. *Phys. Rev. Lett.* **97**, 187401 (2006)
36. Schmucker, S.W., Cress, C.D., Culbertson, J.C., Beeman, J.W., Dubon, O.D., Robinson, J.T.: Raman signature of defected twisted bilayer graphene. *Carbon* **93**, 250–257 (2015)
37. Umair, A., Raza, H.: Controlled synthesis of bilayer graphene on nickel. *Nanoscale Res. Lett.* **7**, 1–5 (2012)
38. Gupta, B., Panda, K., Kumar, N., Melvin, A.A., Dash, S., Tyagi, A.K.: Chemically grafted graphite nanosheets dispersed in poly (ethylene-glycol) by  $\gamma$ -radiolysis for enhanced lubrication. *RSC Adv.* **5**, 53766–53775 (2015)
39. Ferrari, A.C.: Raman spectroscopy of graphene and graphite: disorder, electron–phonon coupling, doping and nonadiabatic effects. *Solid State Commun.* **143**, 47–57 (2007)
40. Lin, J., Wang, L., Chen, G.: Modification of graphene platelets and their tribological properties as a lubricant additive. *Tribol. Lett.* **41**, 209–215 (2011)
41. Chen, B., Bi, Q., Yang, J., Xia, Y., Hao, J.: Tribological properties of solid lubricants (graphite, h-BN) for Cu-based P/M friction composites. *Tribol. Int.* **41**, 1145–1152 (2008)
42. Xu, Y.F., Zheng, X.J., Yin, Y.G., Huang, J., Hu, X.G.: Comparison and analysis of the influence of test conditions on the tribological properties of emulsified bio-oil. *Tribol. Lett.* **55**, 543–552 (2014)
43. Gong, T., Yao, P., Xiao, Y., Fan, K., Tan, H., Zhang, Z., Zhao, L., Zhou, H., Deng, M.: Wear map for a copper-based friction clutch material under oil lubrication. *Wear* **328**, 270–276 (2015)
44. Muthuraja, A., Senthilvelan, S.: Adhesive wear performance of tungsten carbide based solid lubricant material. *Int. J. Refract. Hard Met.* **52**, 235–244 (2015)
45. Major, L., Janusz, M., Kot, M., Lackner, J., Major, B.: Development and complex characterization of bio-tribological Cr/CrN+aC: H (doped Cr) nano-multilayer protective coatings for carbon-fiber-composite materials. *RSC Adv.* **5**, 9405–9415 (2015)
46. Li, X., Zhou, Y., Ji, X., Li, Y., Wang, S.: Effects of sliding velocity on tribo-oxides and wear behavior of Ti-6Al-4 V alloy. *Tribol. Int.* **91**, 228–234 (2015)
47. Allen, M.J., Tung, V.C., Kaner, R.B.: Honeycomb carbon: a review of graphene. *Chem. Rev.* **110**, 132–145 (2009)
48. Wang, L., Zhang, Q., Li, X., Cui, X., Wang, S.: Severe-to-mild wear transition of titanium alloys as a function of temperature. *Tribol. Lett.* **53**, 511–520 (2014)
49. Karlsson, P., Gåård, A., Krakhmalev, P.: Influence of tool steel microstructure on friction and initial material transfer. *Wear* **319**, 12–18 (2014)
50. Berman, D., Erdemir, A., Sumant, A.V.: Few layer graphene to reduce wear and friction on sliding steel surfaces. *Carbon* **54**, 454–459 (2013)
51. Kim, K.-S., Lee, H.-J., Lee, C., Lee, S.-K., Jang, H., Ahn, J.-H., Kim, J.-H., Lee, H.-J.: Chemical vapor deposition-grown graphene: the thinnest solid lubricant. *ACS Nano* **5**, 5107–5114 (2011)
52. Sarno, M., Senatore, A., Cirillo, C., Petrone, V., Ciambelli, P.: Oil lubricant tribological behaviour improvement through dispersion of few layer graphene oxide. *J. Nanosci. Nanotechnol.* **14**, 4960–4968 (2014)
53. Berman, D., Erdemir, A., Sumant, A.V.: Reduced wear and friction enabled by graphene layers on sliding steel surfaces in dry nitrogen. *Carbon* **59**, 167–175 (2013)